Site Preference of Vanadium doped into $ZrSiO_4$ and $ZrGeO_4$ and of Terbium doped into $ZrGeO_4$ *

Peter Chandley,[a] Robin J. H. Clark,[a] Ross J. Angel[b] and G. David Price[b]
[a] *Christopher Ingold Laboratories, University College London, 20 Gordon Street, London WC1H 0AJ, UK*
[b] *Department of Geological Sciences, University College London, Gower Street, London WC1E 6BT, UK*

The site which vanadium prefers to occupy in $ZrSiO_4$ (zircon) and $ZrGeO_4$ and which terbium prefers occupy in $ZrSiO_4$ has been investigated by lattice-energy calculations, electron-probe analysis, and X-ray diffraction. Lattice-energy calculations on pure and doped ZrO_2 and $ZrSiO_4$ using CASCADE computer codes indicate that, although the energies required to substitute V^{4+} for Si^{4+} and Zr^{4+} in each host material are very similar to one another, more distortion of the lattice takes place on substitution for Si^{4+} than for Zr^{4+}. Both electron-probe analysis and X-ray diffraction indicate that vanadium dopes into both the Zr^{4+} and the Si^{4+} sites of $ZrSiO_4$, into the Ge^{4+} site of $ZrGeO_4$, and that terbium dopes into the Zr^{4+} site of $ZrGeO_4$.

On account of its blue colour, high stability and comparatively low cost, vanadium-doped $ZrSiO_4$ (zircon) is important as an inorganic pigment in the ceramics industry.[1,2] Praseodymium-doped zircon is likewise used as a yellow pigment. There is thus considerable interest within the ceramics industry in zircon as a naturally occurring host lattice for a wide variety of potentially dopant ions. Studies have been carried out on the electronic structure of V^{4+},[3-5] Cr^{3+}, Fe^{3+}, Ge^{4+}, Y^{3+}, Nb^{5+}, Mo^{3+}, Pr^{4+}, Nd^{3+}, Eu^{3+}, Gd^{3+}, Tb^{4+}, Dy^{3+}, Er^{3+}, U^{4+} and U^{5+} in zircon. On the basis of their large ionic radii, the rare-earth metal ions M^{3+} are believed to substitute into the Zr^{4+} site in zircon since ionic radii decrease in the order $M^{3+} > Zr^{4+} > Si^{4+}$. However in the case of V^{4+} the existing conclusions are contradictory; ESR and electronic spectral data have been interpreted in favour of substitution of V^{4+} into the Zr^{4+} site only,[3] into the Si^{4+} site only,[4] and into both the Zr^{4+} and the Si^{4+} sites.[5]

The principal problem which arises in electronic spectral studies (regarding whether V^{4+} enters the Zr^{4+} or Si^{4+} sites in zircon) is that both sites have the same (D_{2d}) symmetry. Thus the selection rules and the polarisation of electronic bands originating from V^{4+} ions at each possible site are identical (albeit not the energies, which differ by a factor of two for a given metal–oxygen bond distance according to crystal-field theory, since the Zr^{4+} site is eight-co-ordinate whereas the Si^{4+} is four-co-ordinate). Moreover, it is difficult to assess both the extent of possible lattice distortion and symmetry lowering on substitution and the mechanism by which the dopant ion enters the host lattice.

The aim of this study was to determine the site at which vanadium prefers to be doped in $ZrSiO_4$ and $ZrGeO_4$, and at which site terbium prefers to be doped in $ZrGeO_4$, by the following procedures: (1) lattice-energy calculations, whereby an attempt is made to predict the energetically more stable site in each case; (2) electron-probe analysis of vanadium-doped samples of $ZrSiO_4$ and $ZrGeO_4$ (from the Zr:Si and Zr:Ge ratios it should be evident at which site the vanadium has entered); and (3) refinement of X-ray diffraction data from single crystals of $ZrSiO_4$ and $ZrGeO_4$ doped with vanadium or terbium.

Experimental

Computational Techniques.—(a) *Model potentials.* In order to calculate crystal properties it is essential that the interactions between atoms can be reliably described by model potentials. In ionic and semi-ionic solids the electrostatic coulomb energy forms the major contribution to the cohesive energy, equation (1) where $q_i q_j$ = full or partial charges of the interacting

$$U_{\text{cohesive}}(r_{ij}) = \Sigma_{ij} \frac{q_i q_j}{4\pi\varepsilon_0 r_{ij}} + \Sigma\varphi_{ij}(r_{ij}) + \Sigma\varphi_{ijk}(r_{jk}) \quad \cdots \quad (1)$$

species, r_{ij} = distance between ions i and j, ε_0 = permittivity and φ_{ij} = short-range potential between ions i,j. The short-range forces act between neighbouring ions and arise through the effects of overlap of electron clouds, induction, covalency, *etc.* Pairwise interactions are generally highly repulsive at small values of r_{ij}, and prevent the lattice collapsing in on itself. Many-body forces may be modelled by potentials such as that in equation (2) where θ is the bond angle between ijk, θ_0 is the

$$\varphi_{ijk} = \tfrac{1}{2}K^s(\theta - \theta_0)^2 \quad (2)$$

equilibrium bond angle, and K^s is an harmonic spring constant.

For models in which the electric polarisability is ignored the forces can be described in terms of the electrostatic and short-range interactions. The analytical form of the Born–Mayer–Buckingham potential has been shown theoretically to give a good representation of the short-range interactions between ions [equation (3)]. The parameters A_{ij}, ρ_{ij} and C_{ij} (the

$$\varphi_{ij} = A_{ij}\exp(-r_{ij}/\rho_{ij}) - C_{ij}r_{ij}^{-6} \quad (3)$$

attractive van der Waals term) have to be determined for each pair of ions.

In the presence of an effective electric field, E, at the ion, a distortion of the electron charge cloud will cause an induced dipole moment, μ, at the ion, given by equation (4) where α is the

$$\mu = \alpha E \quad (4)$$

polarisability of the ion. For high frequencies the whole relative permittivity arises in this way. However for low or static frequencies the ions are also displaced, making a contribution to the relative permittivity. The most successful way of incorporating ionic polarisability has been with the shell model of Dick and Overhauser.[6] The massless electron shell, effectively modelling the valence electrons, is given a charge Y and is coupled to the core by a spring constant K. The interaction

* *Non-SI units employed:* eV $\approx 1.60 \times 10^{-19}$ J, dyn $= 10^{-5}$ N.

Table 1 Electron-probe analysis

Lattice	Dopant	Formula	Normalised formula	Code*
$ZrSiO_4$	V^{4+}	$Zr_{1.034}Hf_{0.012}V_{0.043}Si_{0.899}O_4$	$Zr_{0.977}Hf_{0.012}Si_{0.955}V_{0.043}O_4$	Z3
$ZrSiO_4$	V^{4+}	$Zr_{1.040}Hf_{0.014}V_{0.001}Si_{0.944}O_4$	$Zr_{0.983}Hf_{0.012}Si_{1.003}V_{0.001}O_4$	
$ZrSiO_4$	V^{4+}	$Zr_{1.035}Hf_{0.011}V_{0.003}Si_{0.945}O_4$	$Zr_{0.978}Hf_{0.012}Si_{1.004}V_{0.003}O_4$	Z1
$ZrSiO_4$	Cr^{3+}	$Zr_{1.045}Hf_{0.014}Si_{0.941}O_4$	$Zr_{0.988}Hf_{0.012}Si_1O_4$	
$ZrSiO_4$	V^{3+}	$Zr_{1.068}Hf_{0.015}Si_{0.918}O_4$	$Zr_{1.009}Hf_{0.012}Si_{0.975}O_4$	
$ZrSiO_4$	Undoped	$Zr_{1.045}Hf_{0.013}Si_{0.941}O_4$	$Zr_{0.988}Hf_{0.012}Si_1O_4$	
$ZrSiO_4$	Pr^{4+}	$Zr_{1.045}Hf_{0.012}Si_{0.941}O_4$	$Zr_{0.988}Hf_{0.012}Si_1O_4$	
$ZrSiO_4$	Tb^{4+}	$Zr_{1.045}Hf_{0.011}Tb_{0.012}Si_{0.941}O_4$	$Zr_{0.988}Hf_{0.012}Tb_{0.012}Si_{0.933}O_4$	Z2
$ZrGeO_4$	V^{4+}	$Zr_{1.124}Hf_{0.002}V_{0.001}Ge_{0.873}O_4$	$Zr_{0.988}Hf_{0.002}V_{0.001}Ge_1O_4$	
$ZrGeO_4$	V^{4+}	$Zr_{1.120}Hf_{0.001}V_{0.005}Ge_{0.874}O_4$	$Zr_{0.996}Hf_{0.001}V_{0.005}Ge_{1.001}O_4$	
$ZrGeO_4$	V^{4+}	$Zr_{1.136}Hf_{0.000}V_{0.043}Ge_{0.821}O_4$	$Zr_{1.010}Hf_{0.000}V_{0.043}Ge_{0.940}O_4$	S1
$ZrGeO_4$	Tb^{4+}	$Zr_{1.076}Hf_{0.000}Tb_{0.039}Ge_{0.890}O_4$	$Zr_{0.957}Hf_{0.000}Tb_{0.039}Ge_{1.018}O_4$	S2
$HfSiO_4$	V^{4+}	$Hf_{0.968}Zr_{0.016}V_{0.009}Si_{1.003}O_4$		
$HfGeO_4$	V^{4+}	$Hf_{1.107}Zr_{0.025}Ge_{0.863}O_4$		

* Z1, light blue; Z2, yellow; Z3, dark blue; S1, purple; S2, deep red.

between the core (c) and the shell (s) of ion i is then treated as harmonic, equation (5), where r_i is the core–shell separation.

$$\varphi_i^{cs}(r_i) = K_i|r_i|^2 \quad (5)$$

The polarisability is then given by equation (6). Treating the

$$\alpha_i = (Y_i|e|)^2/K_i \quad (6)$$

electron cloud as a separate species allows the ion to distort in an electric field.

(b) *Potentials modelled in this study.* In order to use the potential model it is necessary to obtain values for the constants A, ρ, C, K and Y. The potential terms for Zr–O, V–O and Si–O interactions have been calculated by empirical methods, *i.e.* by optimising potential parameters to give the best description of crystal properties such as elastic and dielectric constants, lattice parameters, and the frequencies of phonon modes. The O • • • O short range parameters used in this study were derived theoretically by Hartree–Fock methods.[7] There has been much work in simulating the potentials of silicates,[8] and the Si–O potential used in this study, derived by Sanders *et al.*,[9] included a three-body term to model the directionality of the O–Si–O angle. A Zr–O potential was derived by Lewis and Catlow,[10] but it proved necessary to use a more recently derived[11] potential in this study. Lewis and Catlow's Zr–O potential had been fitted to cubic or tetragonal phases when in fact the low-temperature phase studied in this work is monoclinic. Thus the Zr–O potential used in the simulation of pure and doped ZrO_2 has been specially derived[11] to describe the seven-co-ordinated zirconium in this phase. The V–O potential adopted was that used successfully to model VO_2 and VO_2 (B).[12] The set of parameters used in this study is listed in Table 4.

The lattice energies evaluated in this study were calculated using the code PARAPOCS[13] by minimising both internal and external strains at 0 K. From the lattice-energy calculations one can go on to evaluate other lattice properties such as unit-cell parameters, elastic constants, bulk moduli and relative permittivities. From these values an estimate of the accuracy or suitability of the model potential can be made.

(c) *Defect calculations.* The aim of the defect calculations is to simulate lattice relaxation around a point defect and to use this to evaluate the energy of formation of the defect, the property calculated being $dU_v = u_v$, the change in internal energy at constant volume. The energies are scaled such that the internal energy of a perfect crystal becomes zero, and hence the energy required to remove a bulk lattice ion to infinity is always positive. The code CASCADE[14] was used to calculate defect energies; it uses the Mott–Littleton approximation[15] to provide an estimate of the interaction between the defect and the infinite perfect lattice.

Electron-probe Analyses.—A variety of doped $ZrSiO_4$, $HfSiO_4$, $ZrGeO_4$ and $HfGeO_4$ crystals, synthesised by flux methods,[16] were subjected to electron-probe analysis by Dr. Steven Reed of the Earth Sciences Laboratory, Cambridge (Table 1). All the samples analysed were set in a 20 × 35 × 5 mm Araldite block and polished with 1 μm diamond paste. Each crystal was analysed in at least two places with the probe in the wavelength-dispersive mode. All the crystals were analysed for content of Pb, Mo, Cr, Na, V, Zr, Si, Ge, Hf, Tb and Pr. Concentrations of impurities could be measured down to 0.02% molar and the counting time for V was increased so that it could be measured at levels greater than 0.01% molar. The concentrations of the various metal ions in each material were measured by reference to a metal standard. Owing to the differences between the diffraction properties of these standards and of the metal ions present in the crystals the concentrations of Zr^{4+} appear too high and those of Si^{4+} and Ge^{4+} too low. This problem was dealt with by normalising the concentrations of Zr, Si and Ge with respect to those in the pure crystals on assumption of 1:1 Zr:Si and Zr:Ge ratios.

X-Ray Diffraction.—A number of crystals was selected from those grown by flux methods for analysis by single-crystal X-ray diffraction. All the crystals used displayed tetragonal morphology and uniform extinction in transmitted polarised light. No inclusions, bubbles or cracks were observed in the crystals, which were broken up into fragments small enough for examination.

All the data sets were collected at room temperature using a Picker four-circle diffractometer equipped with a conventional sealed tube providing Mo-Kα radiation (λ = 0.7107 Å). Unit-cell parameters were determined by least-squares fitting of the positions of 20 reflections in the range $44 < 2\theta < 70°$ centred by the method of King and Finger[17] to eliminate the effect of offset errors and diffractometer aberrations. The unconstrained cell parameters of all crystals exhibited tetragonal symmetry within the estimated standard deviations (e.s.d.s); cell parameters constrained to tetragonal symmetry are listed in Table 2. With the exception of sample Z3 the unit-cell parameters of all of the samples show no significant variation and are in good agreement with values previously reported for $ZrSiO_4$ (Robinson *et al.*,[18] Hazen and Finger[19]) and $ZrGeO_4$ (Ennaciri *et al.*[20]).

Symmetry-allowed data with $0 < 2\theta < 80°$ were collected with ω-step scans, with $-11 \leqslant h \leqslant +11, -11 \leqslant k \leqslant +11$ and $0 \leqslant l \leqslant 10$ (eight asymmetric units) for the $ZrSiO_4$ crystals and $-8 \leqslant h \leqslant +8$, $-8 \leqslant k \leqslant +8$ and $0 \leqslant l \leqslant 17$ (four asymmetric units) for the $ZrGeO_4$ crystals. Intensity and orientation standards were recorded every 3 h; the intensities were found to vary by less than 1% for all the crystals examined.

Table 2 Cell parameters

Data set	a/Å	c/Å	V/Å	c/a
$ZrSiO_4$				
Z1	6.6042(2)	5.9808(2)	260.85(2)	0.9056
Z3	6.6063(2)	5.9832(3)	261.12(2)	0.9057
$ZrGeO_4$				
S1	4.865(1)	10.538(2)	249.5(1)	2.1661
S2	4.8681(3)	10.5470(7)	249.95(4)	2.1665

Table 3 Data collection details for data sets Z1, Z3, S1 and S2

	Z1	Z3	S1	S2
Total no. of symmetry-allowed reflections	1526	1497	1551	1552
No. of reflections with $I > 1.5\sigma_I$	1464	1450	1122	1194
Total no. of independent reflections	227	228	391	391
No. of independent reflections with $F > 3\sigma_{(F)}$	219	218	260	284
Density/g cm^{-3}	4.67	4.66	6.06	6.05
Absorption coefficient/cm^{-1}	43.92	43.88	157.88	157.59
Transmission coefficients	0.25–0.52	0.52–0.71	0.35–0.65	0.10–0.50
Agreement indices for averaging				
All reflections				
F	2.33	1.76	5.54	4.72
F^2	4.62	3.38	7.12	6.31
$F > 3\sigma_{(F)}$				
F	2.26	1.65	3.79	3.54
F^2	4.62	3.36	6.91	6.19

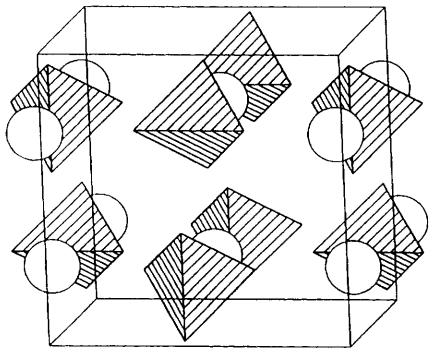

Fig. 1 Polyhedron representation of the structure of $ZrSiO_4$; the circles represent Zr atoms

The step scans were integrated using a Lehman–Larsen algorithm to set the backgrounds and an option to set these interactively. Psi scans indicated the presence of absorption and extinction effects in all of the crystals. Corrections for absorption were made using the program of Burnham.[21] Data were averaged in point groups $4/mmm$ for $ZrSiO_4$ and $4/m$ for $ZrGeO_4$. Internal agreement indices for averaging are given in Table 3. In the refinements a weight of $w = [\sigma^2(F_o) + kF_o^{-2}]^{-1}$ was assigned to each reflection, where $\sigma(F_o)$ is the e.s.d. derived from counting statistics and $k = 0.01$. Initial parameters for the refinements were taken from Robinson *et al.*[18] for $ZrSiO_4$ and from Ennaciri *et al.*[20] for $ZrGeO_4$. The scale factor, the extinction coefficient, and positional and thermal parameters were refined using a locally modified version of RFINE 4.[22] Extinction coefficients were corrected for all crystals using the Becker and Coppens formalism[23] (isotropic Lorentzian type I distribution). All refinements were terminated when the average least-squares shift/e.s.d. of all refined parameters was 0.005, with the maximum shift of any parameter being 0.02 e.s.d. Complex atomic scattering factors were taken for neutral atoms from the ref. 24. Details of the results of the refinements for the four most significant data sets are given in the next section.

Table 4 Lattice calculation data

Potential parameters

	A/eV	ρ/Å	C/eV Å^{-6}	Ref.
Zr–O	985.869	0.3760	0.0000	10, 11
Si–O	1283.900	0.3205	10.6600	9
V–O	640.690	0.4043	0.0000	12
O···O	22 764.000	0.1490	27.8900	7

Shell model parameters

Interaction	Shell charge (Y/e)	Spring constant (K/eV)
O(core)···O(shell)	−2.077	27.290
Three-body terms	K_s/eV	θ_0/°
O–Si–O	2.09	109.54

Lattice energies

Lattice	Energy/eV	Lattice	Energy/eV
$ZrSiO_4$	−238.62	VO_2	−111.05
ZrO_2	−109.88	SiO_2	−128.60

Crystal lattice parameters *

Lattice	a/Å	b/Å	c/Å	U/Å^3	β/°
$ZrSiO_4$	6.612	6.612	5.994	262.00	90
	(6.432)	(6.432)	(6.223)	(257.53)	(90)
ZrO_2	5.138	5.204	5.313	142.05	99.2
	(5.108)	(5.084)	(5.671)	(147.24)	(98.6)
VO_2	4.540	4.540	2.880	59.36	90
	(4.539)	(4.539)	(3.214)	(66.24)	(90)

Elastic constants ($c_{ij} \times 10^{11}$ dyn cm^{-2}) for $ZrSiO_4$*

c_{11}	c_{33}	c_{44}	c_{12}	c_{31}
42.3	49.0	11.3	7.3	14.9
(34.5)	(55.0)	(9.2)	(7.9)	(19.3)

* Calculated values in parentheses.

Table 5 Defect energies (eV)

Defect	Relaxed energy	Unrelaxed energy
$ZrSiO_4$		
Vacancy, V		
Zr^{4+}	85.41	123.00
Si^{4+}	105.81	163.73
O^{2-}	24.31	25.70
Substitution		
V_{Zr}	0.84	0.99
V_{Si}	16.81	19.17
ZrO_2		
Vacancy, V		
Zr^{4+}	85.42	136.57
$O(1)^{2-}$	18.49	34.16
$O(2)^{2-}$	17.80	33.93
Substitution		
V_{Zr}	−1.51	−1.02

Table 6 Calculated bond lengths (Å) for substitution of vanadium onto the Zr^{4+} site

Metal ion	Anion	Distance	
V^{4+}	O(1),O(2),O(3),O(4)	2.04	Axial
	O(5),O(6),O(7),O(8)	2.276	Equatorial
Zr^{4+}(1,2,3,4)	O	2.100	Axial
	2 × O	2.118	Axial
	O	2.129	Axial
	O	2.252	Equatorial
	2 × O	2.269	Equatorial
	O	2.309	Equatorial
Zr^{4+}(5,6,7,8)	2 × O	2.114	Axial
	2 × O	2.117	Axial
	2 × O	2.271	Equatorial
	2 × O	2.272	Equatorial
Si^{4+}(1,2)	2 × O	1.628	Bonded to V^{4+}
	2 × O	1.635	
Si^{4+}(3,4,5,6)	2 × O	1.632	
	2 × O	1.636	

Table 7 Calculated bond lengths (Å) upon vanadium substitution onto the Si^{4+} site

Metal ion	Anion	Distance	
V^{4+}	O(1),O(2),O(3),O(4)	1.758	
Zr^{4+}(1,2)	2 × O	2.122	Axial bonded to V^{4+}
	2 × O	2.153	Axial
	2 × O	2.232	Equatorial
	2 × O	2.246	Equatorial
Zr^{4+}(3,4,5,6)	O	2.070	Axial bonded to V^{4+}
	O	2.106	Axial
	2 × O	2.116	Axial
	O	2.247	Equatorial
	O	2.296	Equatorial
	2 × O	2.299	Equatorial
Si^{4+}(1,2,3,4)	O	1.625	Bonded to V^{4+}
	2 × O	1.634	
	O	1.637	
Si^{4+}(5,6,7,8)	2 × O	1.632	
	2 × O	1.633	

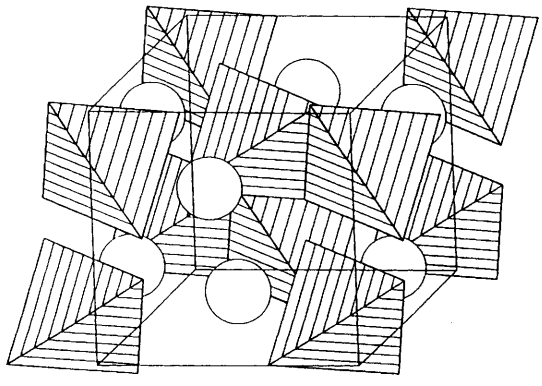

Fig. 2 Polyhedral representation of the structure of $ZrGeO_4$; the circles represent Zr atoms

Results and Discussion

Computer Simulation.—Perfect lattice and defect calculations. The calculated lattice energies and physical properties of $ZrSiO_4$, ZrO_2, VO_2 and SiO_2 are listed in Table 4.[25–29]

The energies required to create Zr^{4+} and Si^{4+} vacancies in the host materials $ZrSiO_4$ and ZrO_2 and to substitute vanadium for Zr^{4+} in ZrO_2 and $ZrSiO_4$ as well as vanadium for Si^{4+} in $ZrSiO_4$ are listed in Table 5. The calculated V–O, Si–O and Zr–O bond lengths for vanadium substitution into the Zr^{4+} site in $ZrSiO_4$ are listed in Table 6 (Fig. 1), and the corresponding bond lengths for vanadium substitution into the Si^{4+} site in $ZrSiO_4$ are listed in Table 7 (Fig. 2). The possibility that vanadium may occupy an interstitial site in $ZrSiO_4$ was checked by placing the vanadium ion in an interstitial site and then relaxing the lattice, but in each case the lattice relaxed until the vanadium ion had migrated into the vacant lattice site.

Lattice site preference. There are several ways to address the problem of substitution of V^{4+} into $ZrSiO_4$, depending upon which mode of synthesis is being analysed. In the case of flux-grown crystals of $ZrSiO_4$ the most simple analysis involves the assessment of the relative substitutional energies of V^{4+} into the Zr^{4+} and Si^{4+} sites. These values are given in Table 5 and show that V^{4+} would substitute more easily for Zr^{4+} than for Si^{4+}. However, syntheses of $ZrSiO_4$ involving essentially solid-state processes will require the analysis of defect reactions such as those in Schemes 1 and 2. Using the lattice energies in Table 4 and the substitution energies in Table 5, the energy for Scheme 1

$$VO_2(s) \longrightarrow V^{4+}(g) + 2O^{2-}(g)$$

$$V^{4+}(g) + x(ZrSiO_4)(s) \longrightarrow Zr_{x-1}VSi_xO_{4x}(s) + Zr^{4+}(g)$$

$$Zr^{4+}(g) + 2O^{2-}(g) \longrightarrow ZrO_2(s)$$

Scheme 1

$$VO_2(s) \longrightarrow V^{4+}(g) + 2O^{2-}(g)$$

$$V^{4+}(g) + x(ZrSiO_4)(s) \longrightarrow Zr_xSi_{x-1}VO_{4x}(s) + Si^{4+}(g)$$

$$Si^{4+}(g) + 2O^{2-}(g) \longrightarrow SiO_2(s)$$

Scheme 2

(V^{4+} substituting for Zr^{4+} in $ZrSiO_4$) is calculated to be 2.01 eV, while that for V^{4+} substituting for Si^{4+} (Scheme 2) is −0.74 eV. This suggests that, in a straightforward solid-state reaction between $ZrSiO_4$ and VO_2, V^{4+} could substitute easily for Si^{4+}. In reality, however, $ZrSiO_4$ is not formed by reaction of a V^{4+}-bearing melt with $ZrSiO_4$, but rather by reaction of doped ZrO_2 with SiO_2. The incorporation of V^{4+} into $ZrSiO_4$ is therefore dependent on the defect reaction in Scheme 3. Again by use of

$$VO_2(s) \longrightarrow V^{4+}(g) + 2O^{2-}(g)$$

$$V^{4+}(g) + x(ZrO_2)(s) \longrightarrow Zr_{x-1}VO_{2x}(s) + Zr^{4+}(g)$$

$$Zr^{4+}(g) + 2O^{2-}(g) \longrightarrow ZrO_2(s)$$

Scheme 3

values given in Tables 4 and 5, the energetics of this reaction can be evaluated to be −0.34 eV, thus showing that V^{4+} can be readily taken up into the ZrO_2 lattice.

In conclusion, therefore, depending on the chemical environment present during the synthesis of $ZrSiO_4$, V^{4+} can be readily substituted either for Zr^{4+} (*via* direct substitution or *via* ZrO_2 doping) or for Si^{4+} (*via* Scheme 2).

Lattice-site distortion. The effect of doping vanadium into the zirconium site is to shorten the four equatorial metal–oxygen bonds and to lengthen the four axial metal–oxygen bonds. The lattice compensates for this by moving the relevant silicon and zirconium ions and slightly altering their metal–oxygen bond lengths (Tables 6 and 7). The net change at the dopant-ion site after substitution is that the equatorial oxygen atoms are moved 0.08 Å closer to the metal ion, altering the lattice-ion bond distances from 2.12 (Zr–O) to 2.04 Å (V–O).

The effect of doping vanadium onto the silicon site is that the four oxygen atoms bonded to the vanadium ion move away from their original positions, altering the lattice ion to oxygen bond lengths from 1.63 (Si–O) to 1.75 Å (V–O), a difference of

Table 8 Refinement indices from X-ray refinements

Sample	[8] Site	[4] Site	R	R'	G_{fit}
Z1 *	0.988Zr + 0.012Hf	1.000Si	0.017	0.021	1.63
Z3	0.945Zr + 0.012Hf + 0.043V	1.000Si	0.018	0.039	2.93
Z3 *	0.998Zr + 0.012Hf	0.957Si + 0.043V	0.018	0.039	2.91
S1 *	1.000Zr	0.957Ge + 0.043V	0.036	0.044	2.74
S1	0.957Zr + 0.043V	1.000Ge	0.037	0.044	2.78
S2	1.000Zr	0.961Ge + 0.039Tb	0.047	0.061	3.80
S2 *	0.961Zr + 0.039Tb	1.000V	0.037	0.047	2.94

* Positional and thermal parameters from these structure refinements are reported in Table 9; $R = \Sigma|F_o - F_c|/\Sigma F_o$, $R' = [\Sigma w(|F_o| - |F_c|)^2/\Sigma w F_o^2]^{\frac{1}{2}}$ and $G_{fit} = [\Sigma w(|F_o| - |F_c|)^2/(N_{obs} - N_{par})]^{\frac{1}{2}}$ where F_o = observed structure factor, F_c = calculated structure factor, w = weight (defined in text), N = No. of observations and N_{par} = number of refined parameters.

Table 9 Positional and thermal parameters from structure refinements

		Sample			
Atom	Parameter	Z1	Z3	S1	S3
Zr	β_{11}	0.001 41(5)	0.0017(1)	0.0024(2)	0.0030(2)
	β_{33}	0.001 31(8)	0.0021(1)	0.000 92(7)	0.000 56(6)
	B_{eq}	0.23	0.30	0.29	0.27
Si or Ge	β_{11}	0.001 61(9)	0.0014(2)	0.0014(2)	0.0023(2)
	β_{33}	0.0013(1)	0.0017(3)	0.000 86(8)	0.000 60(7)
	B_{eq}	0.25	0.24	0.22	0.24
O	x			0.2668(6)	0.2666(6)
	y	0.0660(2)	0.0658(3)	0.1710(7)	0.1711(7)
	z	0.1951(2)	0.1958(3)	0.0815(4)	0.0823(3)
	β_{11}	0.0036(2)	0.0044(4)	0.004(1)	0.006(1)
	β_{22}	0.0021(2)	0.0021(3)	0.0026(9)	0.005(1)
	β_{33}	0.0023(2)	0.0031(4)	0.0016(2)	0.0010(2)
	β_{12}			−0.0008(8)	−0.0004(8)
	β_{13}			−0.0007(4)	−0.0009(4)
	β_{23}	−0.0002(2)	−0.0005(3)	0.0002(5)	−0.0000(4)
	B_{eq}	0.44	0.52	0.45	0.47

In Tables 9 and 10 numbers in parentheses represent estimated standard deviations in the last decimal place quoted. Site occupancies are given in Table 8. In the zircon structure, the following atomic coordinates and anisotropic thermal parameters are fixed: Zr, $x = 0, y = 0.75, z = 0.125, \beta_{22} = \beta_{11}, \beta_{12} = \beta_{13} = \beta_{23} = 0$; Si, $x = 0, y = 0.25, z = 0.375, \beta_{22} = \beta_{11}, \beta_{12} = \beta_{13} = \beta_{23} = 0$; O, $x = 0, \beta_{12} = \beta_{13} = 0$. In the scheelite structure type: Zr, $x = 0, y = 0, z = 0.5, \beta_{22} = \beta_{11}, \beta_{12} = \beta_{13} = \beta_{23} = 0$; Ge, $x = 0, y = 0, z = 0, \beta_{22} = \beta_{11}, \beta_{12} = \beta_{13} = \beta_{23} = 0$.

Table 10 Selected bond lengths (Å) and angles (°) from Z1 and S1 structure refinements *

		Z1	S1
Zr–O	[4]	2.129(1)	2.142(3)
Zr–O	[4]	2.268(1)	2.265(3)
	Average	2.198	2.204
Si(Ge)–O	[4]	1.623(1)	1.765(3)
O–Si–O	[2]	96.95(8)	121.7(4)
O–Si–O	[6]	116.07(4)	103.7(1)

* Bond and angle multiplicities are indicated by numbers in square brackets.

0.12 Å. This is compensated for by moving the zirconium and silicon ions bonded to those oxygen atoms further away from the dopant ion, and by small changes in Zr–O and Si–O bond lengths. Thus the greatest distortion of the lattice on doping occurs with vanadium doping into the Si^{4+} site.

Electron-probe Results.—The results of the electron-probe analyses are shown in Table 1. One satisfactory result is the absence of flux impurities in the samples, which would have had a large effect on the accuracy of the spectroscopic analyses.

In some previous studies of samples where colour was apparent, *e.g.* Cr^{3+}-doped $ZrSiO_4$ (yellow), V^{4+}-doped $HfGeO_4$ (purple), Pr^{4+} in $ZrSiO_4$ (yellow) and in $ZrGeO_4$ (pink), no dopant was detected by the electron probe, *i.e.* the dopant concentration was less than 0.01% (molar) (the origin of the colour centres in the chromium- and vanadium-doped samples had been established to be Cr^{3+} and V^{4+}, by ESR spectroscopy). The doping level of vanadium in $ZrSiO_4$ seems to reach a maximum at 4%. The normalized composition of the $ZrSiO_4$ with the highest concentration of V^{4+} is $Zr_{0.977}Hf_{0.012}Si_{0.955}V_{0.043}O_4$, which suggests that vanadium dopes into the Si^{4+} site, or possibly into both Zr^{4+} and Si^{4+} sites but predominantly the Si^{4+} site. The maximum vanadium doping level measured on $ZrGeO_4$ crystals was 4% but the existence of some deeper coloured crystals suggests that it may be possible to achieve slightly higher levels than this. The $ZrGeO_4$ could also be doped with up to ≈4% Tb^{4+}. The normalised composition of the $ZrGeO_4$ crystal with highest concentration of vanadium, *viz.* $Zr_{1.010}Ge_{0.940}V_{0.043}O_4$, indicates that vanadium enters the Ge^{4+} site. The normalised composition of the $ZrGeO_4$ crystal with the highest concentration of Tb^{4+}, *viz.* $Zr_{0.957}Tb_{0.039}Ge_{1.018}O_4$, suggests that terbium enters the Zr^{4+} site.

The syntheses of vanadium-doped $ZrSiO_4$ and $HfSiO_4$ are almost identical yet the doping levels are 4.3 and 0.9% respectively. This indicates a lower solubility of vanadium in $HfSiO_4$ than in $ZrSiO_4$.

X-Ray Diffraction.—As a preliminary stage of structure refinement each data set was refined with only Zr allocated to the eight-co-ordinate site and Si or Ge, as appropriate, to the tetrahedral site. The phases calculated from the refined models were then combined with the observed structure factors (F_{obs}) to produce electron-density maps of the structures. Careful examination of these maps, including comparison with maps based

upon refinements of data from undoped samples, revealed no evidence of occupancy of interstitial sites by dopant species.

The determination of dopant site was then attempted for each crystal through the comparison of two subsequent refinements. With the Hf allocated to the zirconium site in both cases, the concentration of dopant as determined by microprobe analysis (Table 8) was allocated to the zirconium and tetrahedral sites in turn, and all other structural and thermal parameters were refined. Owing to the way in which occupancies and thermal parameters appear in the structure-factor equation, there is some compensation in the thermal parameters of a given site upon a change in occupancy. This, together with correlations between the thermal parameters and the extinction parameters, reduced the difference between the fit to the data of each pair of structure models. Of the nine samples of $ZrSiO_4$ and $ZrGeO_4$ from which X-ray diffraction data were collected, all but three proved to have doping levels too low to allow the determination of the distribution of the dopant in this way. The results of the structure refinements of these three crystals, together with that of an essentially undoped $ZrSiO_4$ for comparison are reported here.

For zircon Z3, doped with 0.043 V per formula unit, the refinement with V allocated to the tetrahedral site showed a marginal improvement over that with V on the zirconium site. The differences in refinement indices (Table 8) between the two models are not sufficient to exclude the possibility of partial occupancy by V of both sites, but an attempt to refine the distribution of the V directly was unsuccessful due to the correlations with other parameters noted above. Refined positional parameters from each of these refinements show no significant differences, so only those from the refinement with V allocated to the tetrahedral site are reported in Table 9, together with the thermal parameters from the same refinement. Refined parameters for zircon Z1 (0.003 V per formula unit) are provided for comparison. Bond lengths and angles from both of these refinements are the same within the estimated standard deviations, so only those for Z1 are reported in Table 10

The results of the refinements of the two $ZrGeO_4$ scheelite data sets are more definite (Table 8). For the vanadium-doped sample, S1, there is a small but significant improvement in the fit to the data for the model with V allocated to the tetrahedral germanium site. In the case of the terbium-doped sample, S2, the large atomic number contrast allows the Tb to be allocated unambiguously to the zirconium site (Table 8). In both cases these allocations of dopant are supported by the values of the refined thermal parameters. In the accepted models these are consistent with rigid-body behaviour[30,31] of both the GeO_4 and ZrO_8 groups, whereas the rejected models include anomalous parameters which are inconsistent with such behaviour. Final refined parameters for the two accepted models, which represent the first single-crystal structure refinements of $ZrGeO_4$ scheelite, are reported in Table 9, and the bond lengths and angles for S1 are given in Table 10.

Conclusion

The computer simulations and the results of the single-crystal X-ray diffraction studies presented in this paper clearly exclude the possibility of an interstitial mechanism for the substitution of V^{4+} into the $ZrSiO_4$ zircon structure. The results from both of these techniques, and those from the compositional studies by electron microprobe analysis are consistent with the partial substitution of V^{4+} for both Si and Zr. This confirms the predictions of a theoretical analysis,[5] which was based upon electronic data previously collected by Demiray *et al.*[3] and Di Gregorio *et al.*[4] In the case of the scheelite structure of $ZrGeO_4$, the results from electron microprobe analysis of the samples and from single-crystal structure refinement clearly indicate that V substitutes for Ge on the tetrahedral site within the structure, and that Tb substitutes for Zr.

Our results are also in accordance with the distribution of V^{4+} that would be predicted on the basis of a comparison of the ionic radii of the species concerned. Taking radii from Shannon and Prewitt[32] and Shannon,[33] the differences in size between the substituent V^{4+} and the ions in the host lattices are V(8) − Zr(8) = −0.12, V(4) − Si(4) = 0.17 and V(4) − Ge(4) = 0.04 Å. (The radius for V^{4+} in tetrahedral co-ordination has been estimated from systematics in radii for V in a number of co-ordinations and oxidation states.) These simple calculations demonstrate that the germanium tetrahedral site in $ZrGeO_4$ is the best match in terms of size for a V^{4+} substituent, and that the misfit between V^{4+} and the two sites in $ZrSiO_4$ is similar. In the case of terbium substitution into $ZrGeO_4$ the difference between the radius[32,33] or Zr and Tb is only 0.04 Å, indicating a strong crystal chemical preference for substitution on the eight-co-ordinated site of the structure.

Acknowledgements

The authors thank Miss Kate Wright for help with the computer simulation and Dr. Steven Reed for the electron-probe analysis. Cooksons plc and the SERC are thanked for financial support (to P. C.). Diffractometry facilities at the University College London Crystallography Unit are maintained with the support of the Royal Society and NERC.

References

1 C. A. Seabright, *Br. Pat.*, 625, 448, 1949; A. A. Balman and R. A. Laudise, *J. Am. Ceram. Soc.*, 1965, **48**, 130; R. Carter, *Ceram. Ind. J.*, 1985, 19.
2 F. T. Booth and G. N. Peel, *Trans. Br. Ceram. Soc.*, 1962, **61**, 359.
3 T. Demiray, D. K. Nath and F. A. Hummel, *J. Am. Ceram. Soc.*, 1970, **53**, 1.
4 S. Di Gregorio, M. Greenblatt, J. H. Pifer and M. D. Sturge, *J. Chem. Phys.*, 1982, **76**, 2931.
5 H. Xiaoyo, B. Gui-ru and Z. Min-guang, *J. Phys. Chem. Solids*, 1985, **46**, 719.
6 B. G. Dick and A. W. Overhauser, *Phys. Rev.*, 1958, **112**, 90.
7 C. R. A. Catlow, *Defects in Solids: Modern Techniques*, Plenum, New York, 1986, pp. 264–302.
8 S. C. Parker, Ph.D. Thesis, University of London, 1983.
9 M. J. Sanders, M. Leslie and C. R. A. Catlow, *J. Chem. Soc., Chem. Commun.*, 1985, 1271.
10 G. V. Lewis and C. R. A. Catlow, *J. Phys. C*, 1985, **18**, 1149.
11 I. A. Dwivedi and A. N. Cormack, *J. Solid State Chem.*, 1989, **79**, 218.
12 C. R. A. Catlow, A. N. Cormack and F. Theobald, *Acta Crystallogr., Sect. B*, 1984, **40**, 195.
13 G. D. Price, A. Wall and S. C. Parker, *Philos. Trans. R. Soc. London, Ser. A*, 1989, **328**, 391.
14 M. Leslie, Daresbury Laboratory Report DL/SCI/TM 31T, 1982.
15 N. F. Mott and M. J. Littleton, *Trans. Faraday Soc.*, 1938, **34**, 485.
16 P. Chandley and R. J. H. Clark, *J. Crystal Growth*, 1992, **116**, 151.
17 H. E. King and L. W. Finger, *J. Appl. Crystallogr.*, 1979, **12**, 374.
18 K. Robinson, G. V. Gibbs and R. H. Ribbe, *Am. Mineral.*, 1971, **56**, 782.
19 R. M. Hazen and L. W. Finger, *Am. Mineral.*, 1979, **64**, 196.
20 A. Ennaciri, D. Michel and M. Perez y Jorba, *Mater. Res. Bull.*, 1984, **19**, 793.
21 C. W. Burnham, *Am. Mineral.*, 1966, **51**, 159.
22 L. W. Finger and E. Prince, *Nat. Bur Stand. (U.S.), Tech. Note*, 1974, 854.
23 P. J. Becker and P. Coppens, *Acta Crystallogr., Sect. A*, 1974, **30**, 129.
24 *International Tables for X-Ray Crystallography*, Kynoch Press, Birmingham, 1974, vol. 4.
25 V. Butler, C. R. A. Catlow and B. E. Fender, *Radiat. Eff.*, 1983, **73**, 273.
26 H. D. B. Jenkins, *Rev. Chim. Miner.*, 1979, **16**, 134.
27 D. K. Smith and H. W. Newkirk, *Acta Crystallogr.*, 1965, **18**, 983.
28 I. Kawada, N. Kimizuka and M. Nakahira, *J. Appl. Crystallogr.*, 1971, **4**, 343.
29 H. Ozkan, L. Cartz and J. C. Jamieson, *J. Appl. Phys.*, 1974, **45**, 556.
30 R. T. Downs, G. V. Gibbs, M. B. Boisen, *Am. Mineral.*, 1990, **75**, 1253.
31 H. B. Burghi, *Acta Crystallogr., Sect. B*, 1989, **45**, 383.
32 R. D. Shannon and C. T. Prewitt, *Acta Crystallogr., Sect. B*, 1969, **25**, 925.
33 R. D. Shannon, *Acta Crystallogr., Sect. A*, 1976, **32**, 751.

Received 12*th December* 1991; *Paper* 1/06240I